Radiol med (2018) 123:36–43
https://doi.org/10.1007/s11547-017-0808-9

ONCOLOGY IMAGING

Heterogeneity analysis of diffusion-weighted MRI for prediction and assessment of microstructural changes early after one cycle of induction chemotherapy in nasopharyngeal cancer patients

Manijeh Beigi[1] · Anahita Fathi Kazerooni[1] · Mojtaba Safari[1] · Marzieh Alamolhoda[2] · Mohsen Shojaee Moghdam[3] · Shiva Moghadam[4] · Hamidreza SalighehRad[5] · Ahmad Ameri[4]

Received: 6 April 2017 / Accepted: 4 September 2017 / Published online: 15 September 2017

Abstract
Purpose To evaluate whether the pretreatment apparent diffusion coefficient (ADC) heterogeneity parameters and their alterations, after one cycle of induction chemotherapy, can be used as reliable markers of treatment response to induction chemotherapy in patients with nasopharyngeal cancer.
Materials and methods Ten patients were recruited and received induction chemotherapy (IC). Diffusion-weighted imaging was performed prior to, during, and after IC. The first-order ADC histogram parameters at the intra-treatment time-point were compared to the baseline time-point in the metastatic lymph nodes (LNs). Some ADC pretreatment parameters were combined with each other, employing discriminant analysis to achieve a feasible model to separate the complete response (CR) from the partial response (PR) groups.
Results For ten patients, significant rise in Mean and Txt_1Mean ($p = 0.048$ and 0.015, respectively) was observed in the metastatic nodes following one cycle of IC. Txt_5Energy significantly decreased ($p = 0.002$). Discriminant analysis on pretreatment parameters illustrated that $Txt_5Energy_{pre}$ was the best parameter to use to correctly classify CR and PR patients. This was followed by $Txt_9Percentile75_{pre}$, Txt_1Mean_{pre}, and Txt_2Standard $Deviation_{pre}$.
Conclusions Our results suggest that heterogeneity metrics extracted from ADC-maps in metastatic lymph nodes, before and after IC, can be used as supplementary IC response indicators.

Keywords Nasopharyngeal cancer · Lymph node · Induction chemotherapy · Diffusion-weighted MRI

Introduction

Nasopharyngeal carcinoma (NPC) originates from epithelium of the nasopharynx. Approximately two-thirds of NPC cases present with involved regional lymph nodes

✉ Ahmad Ameri
a_ameri@sbmu.ac.ir

Manijeh Beigi
beigi310@gmail.com

Anahita Fathi Kazerooni
anahita.fathi@gmail.com

Mojtaba Safari
mojtaba.safari1@gmail.com

Marzieh Alamolhoda
marzieh_alamolhoda@yahoo.com

Mohsen Shojaee Moghdam
Shojae.mohsen@gmail.com

Shiva Moghadam
moghadamshiva@yahoo.com

Hamidreza SalighehRad
h-salighehrad@tums.ac.ir

1 Quantitative MR Imaging and Spectroscopy Group, Research Center for Cellular and Molecular Imaging, Institute for Advanced Medical Imaging, Tehran University of Medical Sciences, Tehran, Iran

2 Department of Biostatistics, Shiraz University of Medical Science, Shiraz, Iran

3 Payambaran Imaging Center, Tehran, Iran

4 Department of Clinical Oncology, ShahidBeheshti University of Medical Science, Tehran, Iran

5 Department of Medical Physics and Biomedical Engineering, Tehran University of Medical Sciences, Tehran, Iran

[1]. Induction chemotherapy (IC) is an effective treatment decision used to control subclinical metastasis in locally-advanced NPC patients. The use of IC prior to chemo-radiation therapy reduces the rate of distant metastasis, especially for patients with a gap between diagnosis and the start of chemo-radiation therapy [2].

If outcome can be predicted during an early treatment stage, patients could be spared from ineffective treatment toxicity [3–5]. Studies have shown that computed tomography (CT) has a high negative predictive value (NPV) of up to 95%, with a low positive predictive value (PPV) of 35%, for assessing the lymphadenopathy response to chemo-radiation therapy [6]. Ultrasound (US) is preferred for evaluation of intra-nodal architectural changes, but unreliable information of deeper lymph nodes is a major challenge of US [7]. Other imaging modalities (e.g., single photon emission-CT (SPECT) and positron emission tomography (PET)) are limited by low spatial resolution for treatment response, especially shortly after initiation of treatment [8].

Conventionally, assessment of treatment outcome in lymphadenopathy by CT and conventional magnetic resonance imaging (cMRI) is based on measurement of short axis of the lymph nodes, according to RECIST criteria. This method cannot be used within a short duration after the start of treatment, because morphological changes have not occurred yet [9].

Diffusion-weighted (DW) magnetic resonance imaging (MRI) and its derived apparent diffusion coefficient (ADC)-map provide physiological information about tumorous tissues [10]. By quantifying water diffusivity within the tumor, changes in tumor cellularity, which may occur due to chemotherapy, radiotherapy or adjuvant chemo-radiation therapy, can be traced by DWI [10–13].

In this study, a heterogeneity analysis was applied on an ADC-map of the metastatic nodes at the baseline, after one cycle of IC and after two cycles of IC, with the aim of establishing two hypotheses: firstly, pretreatment heterogeneity measures have potential to classify complete response (CR) patients from partial response (PR) patients, and secondly, the alterations of LN's internal microenvironment after one cycle of IC could be detected by the heterogeneity parameters. The present study was performed to test the defined hypotheses in ten patients.

Materials and methods

Patients

Institutional review board (IRB) approval was obtained from the local institution at Shahid Beheshti University of Medical Science for performing serial MRI acquisitions on patients with nasopharyngeal cancer who showed lymph node involvement. Twenty patients with histologically confirmed primary nasopharyngeal cancer who were treated between Jan 2013 and July 2014 at our institution (Jorjani Radiotherapy Center, Imam Hosein Hospital) participated in this study. Among the enrolled patients, 10 patients were excluded for the following reasons: (1) one patient had claustrophobia and could not continue the serial MRI examination; (2) the image quality of three patients was poor and not sufficient for the analysis; (3) two patients didnot have a metastatic lymph node; and (4) four patients decided to continue with their treatment at another institution. Full MR imaging sessions were carried out on the 10 patients who filled out the informed consent form. Table 1 summarizes the patient demographics.

Treatment protocol included two cycles of IC (cisplatin: 75 mg/m^2 in day 1 and 5-FU: 1000 mg/m^2 in days 1–4), followed by a full dose of radiotherapy (70 Gy) to the primary and gross nodal disease and a prophylactic dose to the uninvolved neck regions (60 Gy) using a three-dimensional conformal technique (3DCRT). Radiotherapy was prescribed concurrently with cisplatin (cisplatin: 100 mg/m^2 in days 1 and 29) [4]. Patients were categorized as complete response (CR) patients (with no evidence of disease; $n = 5$) and partial response (PR) patients (with evidence of residual disease or disease relapse; $n = 5$), based on RECIST criteria.

MRI technique and data analysis

MRI protocol

MR imaging was performed on a 1.5 T MRI scanner (Avanto, Siemens Medical Systems, Germany). Conventional images included T1-weighted images (TR/TE = 692/8 ms) and T2-weighted spin-echo images (TR/TE = 4550/116 ms) in axial planes, with slice thickness =6 mm, spacing between slices =6.6 mm, field of view (FOV) =256 × 256 mm^2 and flip angle =90°. Diffusion-weighted images were obtained using a spine echo-planar

Table 1 Patient's demographics

Patient	Age	Sex	Tumor staging	Response
1	44	M	T_2N_3	CR
2	43	M	T_1N_1	PR
3	58	M	T_2N_3	CR
4	33	F	T_2N_1	CR
5	42	M	T_2N_3	CR
6	41	F	T_1N_2	PR
7	49	M	T_1N_2	CR
8	46	M	T_1N_2	PR
9	32	F	T_2N_1	PR
10	32	F	T_2N_2	PR

imaging (EPI) pulse sequence in the axial plane before contrast administration, with slice thickness =5 mm, FOV =192 × 192 mm^2, and TR/TE =1020/88 ms. The diffusion sensitizing gradients were applied in all three orthogonal planes (*X*, *Y*, *Z*) with three *b*-values (0, 500, and 1000) s/mm^2.

Imaging time points were 1 week before, 10 days after the initiation of injection in first cycle of IC and 2 days after the end of second cycle of IC. Clinical MRI sessions were performed every 2 months after the end of chemo-radiation therapy (Fig. 1).

Data analysis and quantification

The largest LNs, which were diagnosed as malignant nodes on a pre-therapeutic clinical and imaging assessment, were identified by an experienced radiologist. The regions of interest (ROI) were then overlaid on the corresponding ADC-maps with a visual guide reference of CE-T_1 images using image-J software at three time points: before treatment (ADC_{pre}), after one cycle of IC (ADC_{intra}), and at the end of IC (ADC_{post}). The ROI masks were extracted and transferred to in-house programs in MATLAB V.7.12 (Math Works Inc.) for further analysis (Fig. 2). In addition, other sets of ROIs were drawn on CE-T_1 images at three time points (i.e., CE-T_{1pre}, CE-T_{1intra}, and CE-T_{1post}) to measure the whole LN volume. Several commonly-used quantitative parameters were calculated on the selected ROIs: mean-, max-, min-, and median-ADC. Furthermore, a first-order histogram texture analysis was performed to spatially quantify the heterogeneity of the metastatic nodes. The parameters were calculated as follows: (1) mean—the mean of the tumor histogram, (2) standard deviation—the average contrast, (3) normalized variance—the measure of smoothness, (4) skewness—the third moment, (5) energy—a measure of uniformity or homogeneity, (6) entropy—a statistical measure of irregularities, (7) kurtosis—the fourth moment, (8) 25th percentile—the smallest scores that are greater than, or equal to 25%, (9) 75th percentile—the smallest scores that are greater than, or equal to 75%, and (10) 95th percentile—the smallest scores that are greater than, or equal to 95%. The definitions of the quantitative parameters (QP) are presented in Table 2.

To assess whether the pretreatment LN volume (LNV) and their changes can be used as a macroscopic predictive marker (based on anatomical images) or not, the entire LN volume was calculated by multiplying the voxel size with the number of voxels, slice thickness, and inter-slice gap within specified ROIs.

Results

QPs were compared between pretreatment (QP_{pre}) and after one cycle of IC (QP_{intra}) using paired sample *t* tests for all patients. A *p* value of less than 0.05 was regarded as statistically significant. The Mean, Txt_1Mean, and Txt_5Energy measures indicated statistically significant differences at $p < 0.05$ (0.048, 0.015 and 0.002, respectively). The evolution of these parameters before, intra (10 days after first injection) and post IC (after the end of two cycle of IC) was depicted for all patients (Fig. 3a, c, e). Parameter changes were evaluated in CR and PR patients, showing that there were no significant differences between the two groups (Fig. 3b, d, f). The reduction in LNV following the first cycle of IC was not significant ($p > 0.05$) (Fig. 3g). The same insignificant downward trend was observed in the CR and PR groups (Fig. 3h).

A positive correlation was observed between Txt_5Energy with LNV_{pre} ($p < 0.047$) (Fig.4). A discriminant analysis was used to build a predictive model, based on a linear combination of the pretreatment parameters that provides the best discrimination between the CR and PR groups. Four parameters (i.e., QPs_{pre}; $Mean_{pre}$, $Txt_5Energy_{pre}$, Txt_2-STD_{pre}, and $Txt_8Percentile75_{pre}$) were combined to determine how well each parameter discriminates between the two groups. The discriminant analysis allowed for the estimation of the linear discriminant function coefficients. Wilks' lambda is a measure of QP's potential, acquired in this analysis process (Table 3). To compare QP_{pre} at different scales, the coefficients of the linear function were standardized.

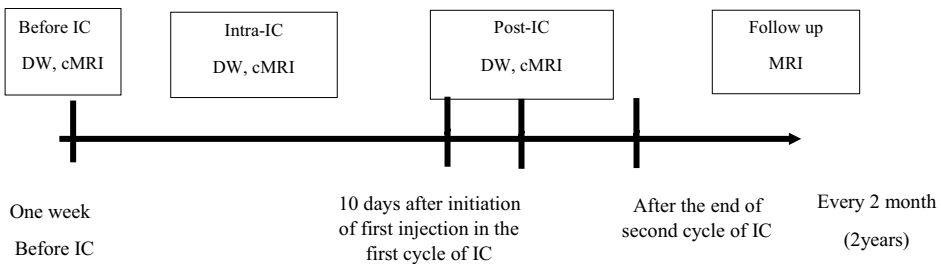

Fig. 1 Timeline of methodological steps in this study

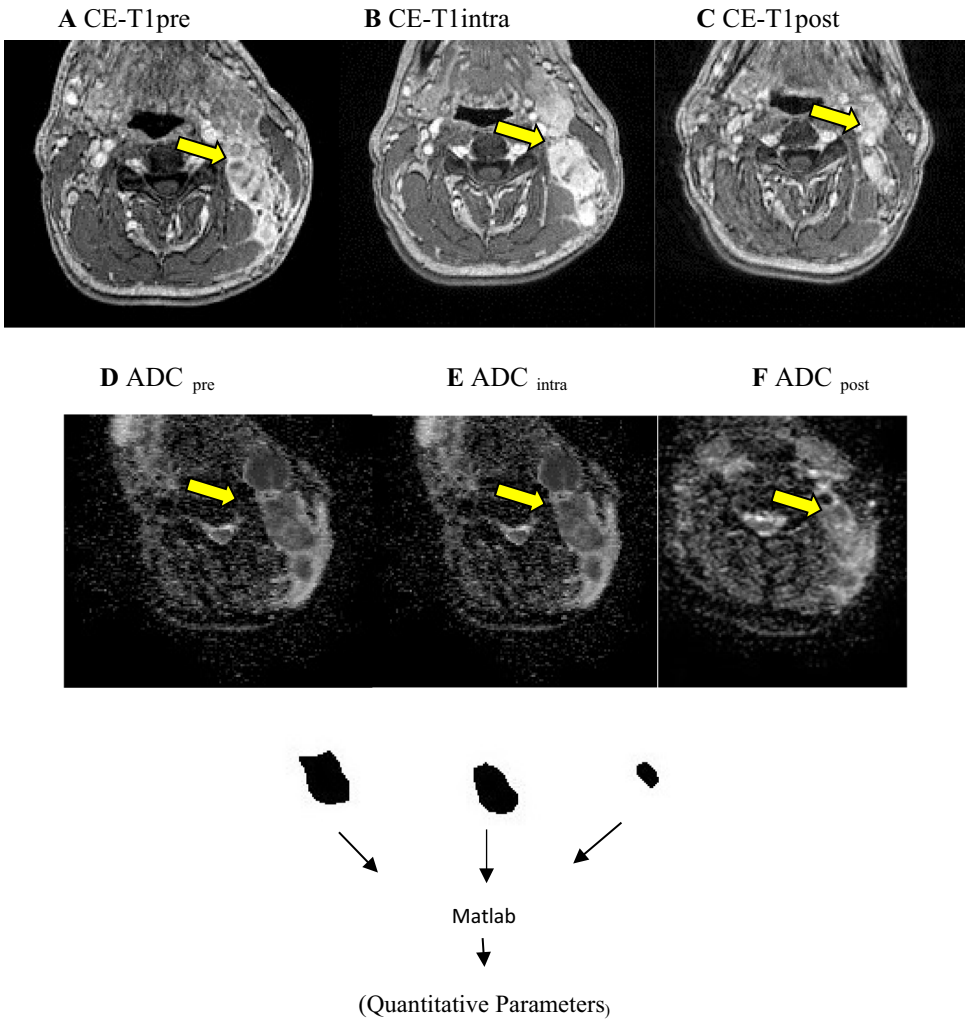

Fig. 2 CE-T_1 images, ADC-maps, and image analysis of a 42 years old patient. Images in each row are from three measurement time points: **a** CE-T_{1pre}, **b** CE-T_{1intra}, **c** CE-T_{1post}, **d** ADC_{pre}, **e** ADC_{intra}, **f** ADC_{post}. Images were windowed to have similar image contrast. The arrows show same nodal metastatic mass that was followed through the treatment course

Discussion

Application of conventional imaging modalities (e.g., CT and MRI) for assessing the lymphadenopathy response to IC is based on LN size, whereas changes in size occur very late or after the end of the IC. Previous studies investigated the role of ADC parameters in predicting the treatment response to therapy in head and neck squamous cell carcinoma (HNSCC) [6, 13]. The study results have shown that the $Mean_{ADC}$ before and during the treatment is useful for assessing the treatment effects. Hatakenaka et al. [2] reported that pretreatment ADC and T-stage are associated with the local failure of chemoradiotherapy or radiotherapy in HNSCC and achieved a significant positive correlation between T-stage and ADC. Sanjeev et al. [14] showed that pretreatment diffusion-weighted and dynamic contrast enhancement metrics of primary tumor and nodal mass are related to the response to treatment. Vandecaveye et al. [6] found that ΔADC in primary lesion and lymphadenopathy 3 weeks after the end of chemoradiotherapy were correlated with tumor recurrence. Changes in the $Mean_{ADC}$ 3 weeks after chemoradiotherapy, in comparison with the corresponding values before treatment, were reported as an indicator for loco-regional failure and loco-regional control by Matoba et al. and Hatakenaka et al. [2, 3].

The results of our study will be discussed from the following two points of view:

Extraction of quantitative texture parameters from the ADC-map for early detection of microstructural changes and treatment response of involved LNs to one cycle of IC

Most investigators extracted the $Mean_{ADC}$ to evaluate the early changes of tumor cellularity. The $Mean_{ADC}$ has some limitations in the evaluation of the response to treatment, due to tumor heterogeneity. Heterogeneity in the ADC signal is based on both tumor cellularity changes, as well as degenerative changes (hemorrhage, cystic or mucinous degeneration). Therefore, the focus of this study was to evaluate

Table 2 Definitions of heterogeneity quantitative parameters

Quantitative parameters	Definition
Mean-ADC	The average of ADC-values within the ROI
Max-ADC	The maximum ADC-value within the ROI
Min-ADC	The minimum ADC-value in the ROI
Median-ADC	The median of ADC-values in the ROI
Txt_1-Mean	The mean of the tumor histogram
Txt_2-STD	The amount of variation from the mean of histogram. This feature is a measure of average contrast within the ROI
Txt_3-NV	The mean of the normalized squared distances of each of ADC-values within the ROI from histogram mean. This feature demonstrates the amount of dispersion of ADC-values around the mean and is a measure of smoothness within the image
Txt_4-Skewness	The amount of asymmetry between values of ADC-values around the mean. If the tail is longer on the left side than the right side, the histogram is negatively skewed and if the right-side tail is elongated, the histogram is positively skewed
Txt_5-Energy	The sum of squared ADC-values within the ROI, which is a measure of homogeneity within the ROI. Higher energy denotes higher homogeneity and lower energy represents heterogeneity
Txt_6-Entropy	The average amount of information within the ROI: more uncertainty requires more information for encoding ad has higher entropy. This measure shows the amount of irregularities within the ROI
Txt_7-Kurtosis	Amount of "peakedness" of the histogram within the ROI. Higher kurtosis reflects more distribution of the values towards the tails rather than the mean and lower kurtosis shows that the ADC-values are more concentrated around the mean
Txt_8-$Percentile_{25}$	The point on the horizontal axis such that 25% of the area under the histogram lies to the left of that point (and 75% to the right)
Txt_9-$Percentile_{75}$	The point on the horizontal axis such that 75% of the area under the histogram lies to the left of that point
Txt_{10}-$Percentile_{95}$	The point on the horizontal axis such that 95% of the area under the histogram lies to the left of that point

metastatic lymph node changes using heterogeneity analysis to reveal their physiological behavior early after one cycle of IC.

In summary, there are two major differences between this ongoing study and the previous studies: first, the use of heterogeneity analysis for LN response assessment, and second, different MRI data acquisition time points and evaluation of response after one cycle of IC. To the best of our knowledge, the employment of texture analysis on ADC-maps for assessing LN's response to just one cycle of IC has yet to be documented. For this purpose, several quantitative metrics were explored to obtain the most accurate feature(s) as potential predictive biomarkers for the early response of the LN to IC. The initial results showed that some of these parameters could detect early changes in the intra-nodal microstructure.

In most studies, effective treatment is reflected by an increase in ADC-values. An elevation of the $Mean_{ADC}$ due to the effects of two cycles of IC or chemo-radiation therapy were investigated by Powell et al. [4], Kim et al. and Chen et al. [13, 15]. However, a significant increase in the Mean and Txt_1Mean of ADC following one cycle of IC was seen in this study. This result concurs with the effective treatment. To investigate the changes of LN's texture after one cycle of IC, heterogeneity parameters were also extracted. Txt_5Energy decreased significantly early after one cycle of IC for all patients, which could be a sign of early changes of the LN internal microenvironment. One must note that the evolution of this parameter over time in CR and PR patients were consistent with the same parameters in all patients. However, there was no correlation between the Mean, Txt_1 Mean, and Txt_5Energy with the CR or PR groups, possibly due to the small number of patients. These results suggest that the previously-mentioned quantitative parameter could be used as a predictive biomarker for the therapeutic response in the early phase (only one cycle of IC) of the treatment in a larger number of patients.

The results of the volumetric measurements were indicative of the inability of LNV's changes to detect a response to one cycle of IC. Significant LNV changes were seen after two cycles of IC. These results agree with those of other studies. In addition, finding the microstructural changes of LN at the cellular level due to only one cycle of IC and using the heterogeneity parameters in this study can be considered a valuable method when visible morphological changes have not occurred yet.

Finding a best combination of pretreatment texture parameters to achieve a model for predicting the response to IC

The correlation of Txt_5Energy with LNVpre for CR and PR groups on a scatter plot was representative of two facts; first, the Txt_5Energy value increased with progression of LNV_{pre}, and second, two CR and PR groups were

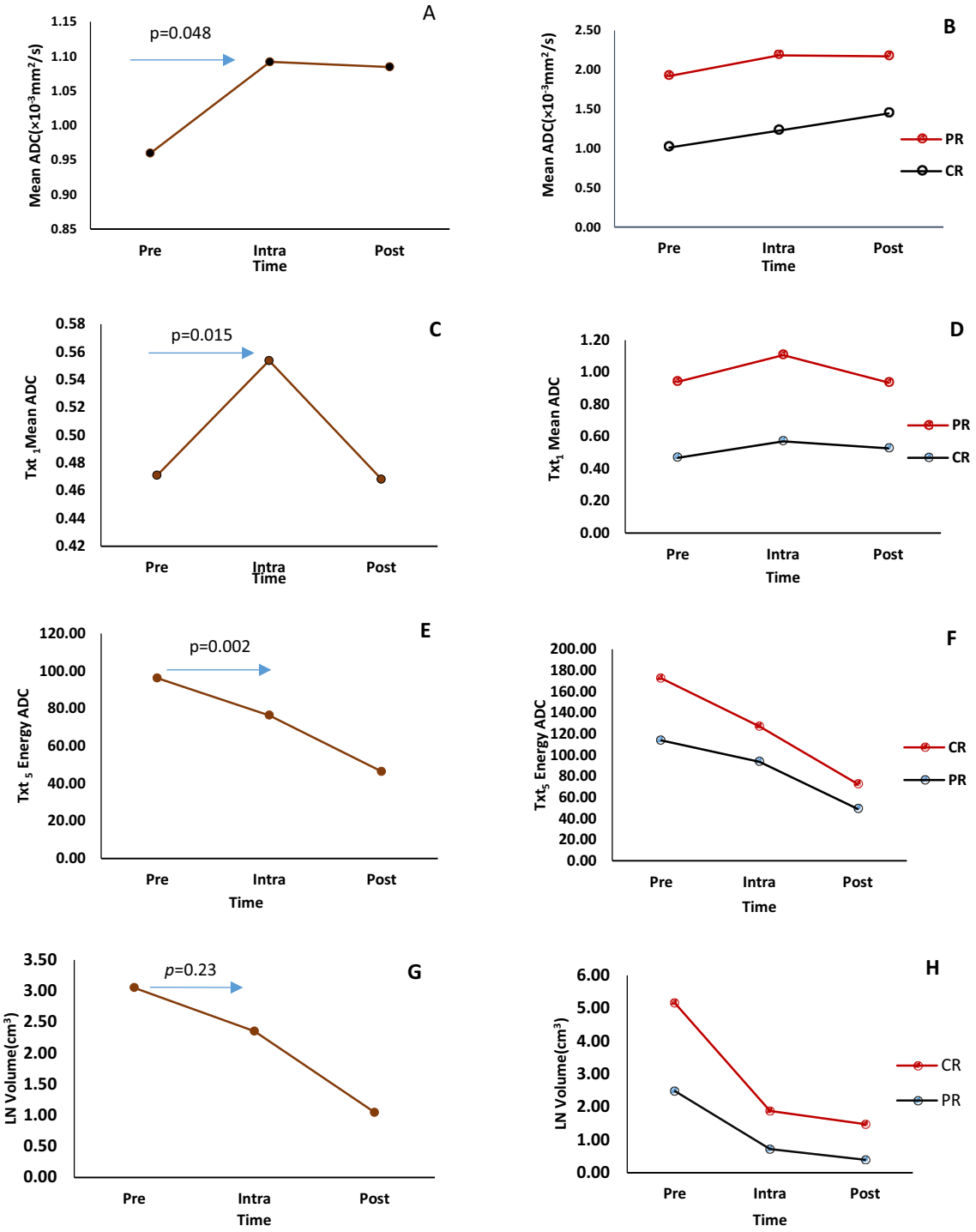

Fig. 3 Comparable evolution in Mean ADC, Txt_1Mean_{ADC}, Txt_5 Energy, and LN Volume following one (intra) and two (post) cycle of IC for all patients (A, C, E, and G), CR and PR patients (B, D, F, and H)

quite distinct from each other, which was indicative of the potential of Txt_5Energy to classify CR from PR group. Based on these results, the best pretreatment parameters to classify CR from PR patients were sought. Discriminant analysis was used to find a linear combination of pretreatment variables to separate the groups. Wilks' lambda values and standardized coefficients indicated the parameters' potentials to discriminate between the two CR versus PR groups. A smaller Wilks' lambda and the coefficients with large absolute values corresponded

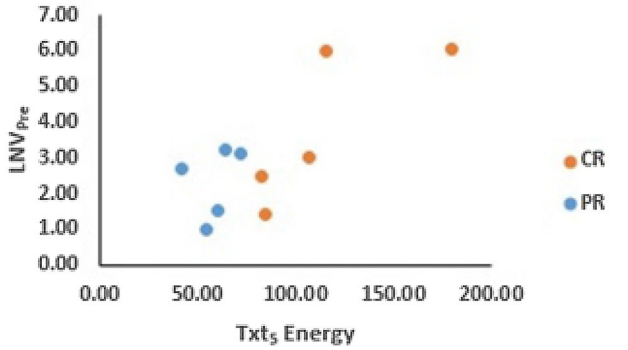

Fig. 4 Significance positive correlation (correlation coefficient: 0.638, $p < 0.05$) between Txt_5 $Energy_{pre}$ and LNV_{pre} Orange and blue circle indicate CR and PR patients

Table 3 Wilk's lambda and standardized coefficients for discriminant model

Quantitative parameters (Pre)	Wilks' lambda	Standardized coif
$Mean_{pre}$	0.798	0.258
Txt_2-Std_{pre}	0.843	−0.221
Txt_5-$Energy_{pre}$	0.467	0.546
Txt_9-$Percentiles75_{pre}$	0.787	−0.266

to parameters with a greater discriminating ability. The Wilks' lambda (Table 3) suggested that $Txt_5Energy_{pre}$ was the best parameter to classify CR from PR patients. This was followed by $percentile75_{pre}$, $Mean_{pre}$, and Sd_{pre}. Therefore, a combination of these parameters was able to correctly classify CR from PR patients with high accuracy.

Our study had some limitations. The sample size was small. However, the results are sufficient to prove that DWI's heterogeneity parameters can assess the early response of neck metastatic nodes to IC. Investigations for a larger patient population will provide more insight into the correlation between heterogeneity parameter alterations and other variables to distinguish the CR from PR group. The author will conduct another study for a larger patient group to confirm the results of this pilot study.

Another limitation was poor quality of DW–MRI in head and neck region. In this study, ROI selection in primary nasopharynx tumor was unsuccessful, due largely to the magnetic field inhomogeneity (susceptibility artifact) at air-bone interfaces. Moreover, degradation of image quality at thoracic inlet regions did not allow for delineation of lymph nodes on ADC-map, for all slices, including the malignant LN. Imaging techniques could be improved using T2 W-BLADE suggested by Ohgiyain et al. [16]. This would result in higher quality images, so a better ROI selection will be possible in all areas of the head and neck for each patient.

Our preliminary results suggest that a heterogeneity analysis on metastatic LN before and early after IC yields valuable information about effect of IC.

Acknowledgements This work was fully supported by a Grant from the Shahid Beheshti University of Medical Science (Grant number: 5232), Tehran, Iran. We are extremely grateful to Ms Aramesh Safari and Mr Pedram Rostami for providing imaging data in Payambaran MRI center. Also, we would like to thank Clinical Research Development Center in Imam Hosein Hospital for highly contributing to the progression of this project.

Compliance with ethical standards

Funding This study was funded by Grant number 5232.

Conflict of interest The authors declare no conflict of interest

Ethical approval All procedures performed in studies involving human participants were in accordance with the ethical standards of the institutional and/or national research committee and with the 1964 Helsinki declaration and its later amendments or comparable ethical standards.

References

1. Wei WI, Sham JS (2005) Nasopharyngeal carcinoma. The Lancet 365(9476):2041–2054
2. Hatakenaka M, Nakrumara K, Yabuchi H et al (2011) Pretreatment apparent diffusion coefficient of the primary lesion correlates with local failure in head-and-neck cancer treated with chemoradiotherapy or radiotherapy. Int J Radiat Oncol* Biol* Phy 81(2):339–345
3. Matoba M, Tuji H, Shimode Y et al (2014) Fractional change in apparent diffusion coefficient as an imaging biomarker for predicting treatment response in head and neck cancer treated with chemoradiotherapy. Am J Neuroradiol 35(2):379–385
4. Powell C, Schmidth M, Marco B et al (2013) Changes in functional imaging parameters following induction chemotherapy have important implications for individualised patient-based treatment regimens for advanced head and neck cancer. Radiother Oncol 106(1):112–117
5. Lee KC, Moffat B, Schott A et al (2007) Prospective early response imaging biomarker for neoadjuvant breast cancer chemotherapy. Clin Cancer Res 13(2):443–450
6. Vandecaveye V, Dirix P, De kazer F et al (2012) Diffusion-weighted magnetic resonance imaging early after chemoradiotherapy to monitor treatment response in head-and-neck squamous cell carcinoma. Int J Radiat Oncol* Biol* Phy 82(3):1098–1107
7. Yoon DY, Hwang H, Chang S et al (2009) CT, MR, US, 18F-FDG PET/CT, and their combined use for the assessment of cervical lymph node metastases in squamous cell carcinoma of the head and neck. Eur Radiol 19(3):634–642
8. Ali TFT (2012) Neck lymph nodes: characterization with diffusion-weighted MRI. Egypt J Radiol Nucl Med 43(2):173–181
9. Eisenhauer E, Therasse P, Bogaerts J et al (2009) New response evaluation criteria in solid tumours: revised RECIST guideline (version 1.1). Eur J Cancer 45(2):228–247
10. King AD, Ahuja A, Yeung D et al (2007) Malignant cervical lymphadenopathy: diagnostic accuracy of diffusion-weighted MR imaging. Radiology 245(3):806–813

11. Hoang JK, Choudhury KR, Chang J, Craciunescu OI, Yoo DS, Brizel David M et al (2014) Diffusion-weighted imaging for head and neck squamous cell carcinoma: quantifying repeatability to understand early treatment-induced change. Am J Roentgenol 203(5):1104–1108
12. Lee MC, Tsai HY, Chung KS, Chen MK et al (2013) Prediction of nodal metastasis in head and neck cancer using a 3T MRI ADC map. Am J Neuroradiol 34(4):864–869
13. Kim S, Loevner L, Quon H et al (2009) Diffusion-weighted magnetic resonance imaging for predicting and detecting early response to chemoradiation therapy of squamous cell carcinomas of the head and neck. Clin Cancer Res 15(3):986–994
14. Chawla S et al (2013) Pretreatment diffusion-weighted and dynamic contrast-enhanced MRI for prediction of local treatment response in squamous cell carcinomas of the head and neck. AJR Am J Roentgenol 200(1):35
15. Chen Y, Liu X, Zheng D et al (2014) Diffusion-weighted magnetic resonance imaging for early response assessment of chemoradiotherapy in patients with nasopharyngeal carcinoma. Magn Reson Imaging 32(6):630–637
16. Ohgiya Y, Suyama J, Seino N et al (2010) MRI of the neck at 3 Tesla using the periodically rotated overlapping parallel lines with enhanced reconstruction (PROPELLER)(BLADE) sequence compared with T2-weighted fast spin-echo sequence. J Magn Reson Imaging 32(5):1061–1067